BEHAVIOURS OF LEADING-EDGE SEPARATION VORTEX FORMED ON A DELTA WING WITH VORTEX FLAPS

Kenichi RINOIE
Department of Aeronautics and Astronautics, University of Tokyo
7-3-1 Hongo, Bunkyo-ku, Tokyo, 113, JAPAN

Toshimi FUJITA, Akihito IWASAKI and Hirotoshi FUJIEDA
National Aerospace Laboratory
6-13-1 Osawa, Mitaka, Tokyo, 181, JAPAN

Abstract

Wind tunnel tests have been made using a 70° delta wing model with leading-edge vortex flaps. The structure of the leading-edge separation vortex over the LEVF was measured by using the 5 holes Pitot probe. The three component velocities, the total pressure, the dynamic pressure and the static pressure distributions over the vortex flap and wing surfaces were measured. By analysing the measured results, characteristics of the leading-edge separation vortices formed both on the delta wing and on the vortex flap are discussed. It is confirmed that the maximum lift/drag ratio for the 70° delta wing is attained, when a separated vortex is formed on the vortex flap and when its spanwise length coincides with the vortex flap spanwise length.

Nomenclature

C	wing centreline chord, m
C_D	drag coefficient
C_L	lift coefficient
Cp	surface pressure coefficient, $(P-P_\infty)/q_\infty$
Cp_D	dynamic pressure coefficient, q_D/q_∞
Cp_S	static pressure coefficient, $(P_S-P_\infty)/q_\infty$
Cp_T	total pressure coefficient, $(P_T-P_\infty)/q_\infty$
L/D	lift/drag ratio
P	surface pressure, N/m^2
P_S	static pressure, N/m^2
P_T	total pressure, N/m^2
P_∞	free stream static pressure, N/m^2
q_D	dynamic pressure, N/m^2
q_∞	free stream dynamic pressure, N/m^2
Re_C	Reynolds number based on the wing centre-line chord
U_∞	free stream velocity, m/s
x	chordwise coordinate measured from the apex of the delta wing, m
y	spanwise coordinate measured from the wing centre line, m
z	coordinate normal to x and y measured from the root chord line, m
α	wing incidence, degree
δ_f	vortex flap deflection angle measured normal to the hinge line, degree

Introduction

The leading-edge vortex flap (LEVF) is the device which can improve the aerodynamic efficiency of delta wings at low speeds[1]. It is a full span deflectable surface at the leading-edge of a delta wing. With the flap deflected downward, a pair of the leading-edge separation vortices is formed over the forward facing flap surfaces (Fig.1). The suction force generated by the vortex acts on the flap and generates a thrust component. Hence it reduces the drag and improves the lift/drag (L/D) ratio, an essential factor for the improvement of the take-off and climb performance of delta wing aircraft. Many tests have been made to confirm the benefit of the LEVF[2].

The authors have made some experimental studies using the delta wing models which have sweepback angles of 50° [3],60° [4] and 70° [5], fitted with tapered LEVFs. Purposes of these studies were to confirm the benefit of the LEVF and to know how the difference of the sweepback angle affects the aerodynamic characteristics of the wing with the LEVF.

Throughout these studies the benefit of the LEVF was confirmed. It was also revealed that the highest lift/drag ratio for the 60° model is achieved using a modest LEVF deflection angle which causes the flow to attach on the flap surface without any large separation[4]. On the contrary, the maximum lift/drag ratio for the 70° delta wing is attained, when a

separated region is formed on the vortex flap and when the spanwise length of this separated region almost coincides with the vortex flap width[5]. The latter results agreed with the observations obtained for the 74° delta wing by Rao[1]. These results suggest that the formation and the behaviour of the leading-edge separation vortex over the LEVF surface should be investigated more in detail, in order to get the maximum understandings of the performance of the LEVF. Therefore, further wind tunnel tests have been made using the 70° delta wing model with the LEVF which was used in Ref.5. The structure of the leading-edge separation vortex over the LEVF was measured by the 5 holes Pitot probe. The three component velocities, the total pressure, the dynamic pressure and the static pressure distributions over the vortex flap surfaces were obtained. By analysing the measured results, the behaviours of the leading-edge separation vortex formed on the LEVF and the effect of the LEVF over the delta wing performance are discussed in this paper.

Experimental Details

Fig.2 shows the model details[5]. The model is a 70° flat plate delta wing with no camber. The center-line chord length C is 0.5m and the thickness is 0.015m. The upper and lower surfaces of all the edges are cut away so that the edges are sharp and have an apex angle of 8.6° at two leading-edges and 12.8° at a trailing-edge, where the angle is measured in a plane normal to the edge concerned. The model has the LEVF hinge lines running from the wing apex to 75% of the trailing-edge semispan station. Three rows of pressure tapping were located on the upper surface and one row on the lower surface. The flap deflection angle δ_f is defined as the angle measured in the plane normal to the hinge line. Flap can be deflected from δ_f=0° to 50°, with an increment of 10°.

The experiments were made in a 2m x 2m low speed, closed working section, closed return wind tunnel at the National Aerospace Laboratory in Japan. All tests were done at a tunnel speed of U_∞= 30m/s. The Reynolds number based on the wing center line chord Re_C was 1×10^6. The three component forces and surface pressure measurements were again made to check the repeatability of the tests. These results agreed well with those of Ref.5.

Flowfield measurements have been made using a 5 holes Pitot probe of 1.8mm diameter. The probe was traversed in planes perpendicular to the freestream direction using the tunnel traversing gear system[6]. The 5 holes Pitot pressure and model surface pressure were measured using Electronically Scanner Pressure Sensors (ESP)[7]. The three component velocities, the total pressure coefficient Cp_T, the dynamic pressure coefficient Cp_D and the static pressure coefficient Cp_S were analysed using the measured data. Because of the restriction of 5 holes Pitot probe, the velocity vector which is declined more than 30° from the free stream direction or which is slower than 10m/s could not be evaluated[7]. The blockage effect of the 5 holes Pitot probe over the model has been checked by measuring the forces and surface pressure distributions, when the probe is traversed near the model surface. The results indicated that the effect of the probe is negligible if the angle of attack of the model is less than 25°.

Results and Discussion

Three Component Forces

Three component force distributions of the 70° delta wing measured in Ref.5 are shown again, to summarize the aerodynamic characteristics of the 70° model tested. The angle of attack α was increased from -10° to 42°. The model was mounted on a shielded strut with a tail sting. To account for interference between the strut and the model, the interference correction using a dummy strut was made in the angle of attack range from -10° to 10°.

The C_L vs. α curves are shown in Fig.3 for various δ_f. Results with strut interference correction are shown in $-10° < \alpha < 10°$ and results without strut interference correction in $\alpha > 10°$. This figure shows that the C_L decreases as the LEVF is deflected downwards. The C_D - α curves (Fig.4) show the C_D decreases for most of the positive α region, as δ_f increases.

Fig.5 shows the lift to drag ratio (L/D) versus C_L. The results with strut interference correction are shown in the C_L range of $C_L \leq 0.4$ and results without the correction in the C_L range of $C_L > 0.4$. A large L/D improvement for δ_f=20° and 30° are seen at about C_L=0.2 ~ 0.3. The observed absolute maximum L/D is 11.8, which is attained at δ_f=20°, α=5°.

Flow Field Measurements (Velocity Vectors)

Fig.6 shows surface pressure distributions for the upper surface at x/C=0.55 at α=5°, plotted against the semi-spanwise station $y/(b/2)$[5]. H.L. denotes the vortex flap hinge position. Results of δ_f=0°, 20° and

50° are shown. The absolute maximum lift drag ratio of 11.8 was attained at this angle of attack for δ_f=20°. Suction regions are seen at $y/(b/2)$=0.75~1.0 for δ_f= 20° and at $y/(b/2)$=0.6~1.0 for δ_f=0°. The spanwise length of the suction region for δ_f=20° is shorter than that for δ_f=0° and almost coincides with the vortex flap spanwise length. The suction region is thought to correspond to the leading-edge separation vortex, as was discussed in Ref.5. For δ_f=50°, the suction region is seen inboard the flap hinge line ($y/(b/2)$=0.5~0.75). This suggests that a separation region is formed inboard the hinge line.

Fig.7 shows the vectors of the velocity component in the plane perpendicular to the freestream direction for the same cases as in Fig.6, measured by the 5 holes Pitot tube. For δ_f=0° (Fig.7a), it is clearly seen that the leading-edge separation vortex is formed on the wing. Its spanwise station almost coincides with that obtained by the surface pressure measurements in Fig.6. The x sign in this figure denotes that the magnitude or the direction of velocity vector has exceeded the measurement accuracy as was denoted in the experimental apparatus section. It is known that a secondary separation vortex is formed inside the leading-edge separation vortex on a delta wing. However, the secondary separation region inside the vortex could not be measured in this tests, because of the limited number of measurement points by the 5 holes Pitot probe.

Fig.7b shows the velocity vector distributions for δ_f= 20°, when the absolute maximum *L/D* is obtained. It is seen that the separation occurs at the leading-edge and the separation vortex is formed. The spanwise length of this separation vortex is almost the same as the vortex flap spanwise length.

Fig.7c shows the results for δ_f=50°. Because of a large flap deflection angle, the 5 holes Pitot probe could not reach to the area over the vortex flap surface. Therefore, the flowfield around the vortex flap for this configuration could not be obtained. This figure shows that a separated region is formed inboard the flap hinge line. The recirculating region between $y/(b/2)$=0.45 and flap hinge line ($y/(b/2)$=0.75) shows a similar flow field pattern to the leading-edge separation vortex formed on a plain delta wing (Fig.7a).

Fig.8 shows surface pressure distributions for the upper surface at α=8°, δ_f=30° for different chordwise stations x/C=0.4, 0.55 and 0.7. Near maximum lift drag ratio of 11.1 was attained at this configuration. This figure shows that almost the same pressure distributions are attained for different chordwise stations, which means that a similar flow exists along the chordwise station over the delta wing at this configuration. The pressure distribution in Fig.8 is similar to the one for δ_f=20°, α=5° in Fig.6. This suggests the existence of the separation vortex over the vortex flap at this configuration.

Fig.9 shows the velocity vector components in the measuring plane at the same configuration as in Fig.8 for x/C=0.4, 0.55 and 0.7. These figures show that the leading-edge separation vortex is formed over the vortex flap. The flow patterns of this separation vortex is the same for different chordwise stations. The flow field patterns of Figs.9 are almost identical to the results of the maximum *L/D* configuration in Fig.7b.

The formations of the leading-edge separation vortex were clearly identified in Figs.7a, 7b and 9. The spanwise lengths of these separation vortices coincide very well with those of the suction regions observed in the surface pressure distributions in Figs.6 and 8. Fig.7b and Fig.9 also confirmed the results in Ref.5 that the absolute or near maximum lift/drag ratio for the 70° delta wing is attained when the separated vortex is formed on the vortex flap and when its spanwise length coincides with the vortex flap span length.

Flow Fields Measurements (Pressures)

Fig.10 shows results of flow field measurements of total pressure isobars Cp_T (Fig.10a), static pressure isobars Cp_S (Fig.10b) and dynamic pressure isobars Cp_D (Fig.10c) for the no flap deflection configuration (δ_f= 0°) at α=5°. The surface pressure distributions for this case was shown in Fig.6 and the velocity vectors in Fig.7a. The total pressure contours in Fig.10a shows that the total pressure losses are observed inside the leading-edge separation vortex between $y/(b/2)$=0.6 and 1.0. This tendency is the same for the leading-edge separation vortex formed on a 76° sharp delta wing at α=20.5°, Re_C=2x10^6 in Ref.8. It is noted that some data near the wing surface have not been measured as stated in Fig.7a. Therefore the isobars inside the leading-edge separation vortex near the wing surface should be treated with caution.

Comparisons between the static pressure isobars in Fig.10b and velocity vectors in Fig.7a show that the minimum Cp_S is attained at the core of the separation vortex. It is seen that the spanwise Cp_S distributions

and the magnitude of Cp_S near the wing surface are similar to the surface pressure distributions in Fig.6. This clearly suggests the upward suction force acting over the delta wing by the leading-edge separation vortex.

The dynamic pressure isobars in Fig.10c shows that the maximum Cp_D is attained slightly above the vortex core position. According to the measured velocity vector distribution data, the streamwise velocity is maximum at this highest dynamic pressure position.

Fig. 11 shows the Cp_T, Cp_S and Cp_D isobars for the 20° flap deflected at α=5°. At this configuration, the maximum lift/drag ratio was attained as noted before. The leading-edge separation vortex is formed on the vortex flap surface as shown in Fig.7b. The separation vortex formed on the vortex flap surface in Fig.11 is much smaller and weaker than the separation vortex on the plain delta wing at the same angle of attack in Fig.10. However, results in Figs. 10 and 11 show similar isobar distributions for Cp_T , Cp_S and Cp_D. This indicates that the separation vortex formed on the vortex flap shows the same characteristics as those of the leading-edge separation vortex formed on a plain delta wing. Fig. 11b shows that the minimum static pressure is attained at the core position of the separation vortex. This also confirms the idea by Rao[1] for a slender delta wing that the upward suction force acts on the vortex flap surface, that the drag force acting on the wing decreases and that the lift/drag ratio is consequently increased for the LEVF wing.

Conclusions

Measurements were made on a 70° delta wing with leading-edge vortex flaps using a 5 holes Pitot tube. Velocity vectors, total pressure, static pressure and dynamic pressure distributions over the wing and flap surfaces were obtained.

1) Separation vortices formed on a plain delta wing, on a vortex flap and inboard the vortex flap hinge line were clearly identified.

2) It was confirmed that the maximum lift/drag ratio for the 70° delta wing is attained, when a separated vortex is formed on the vortex flap and its spanwise length coincides with the vortex flap spanwise length.

3) According to the total, static and dynamic pressure measurements inside the vortices, the leading-edge separation vortex formed on the vortex flap shows similar characteristics to the one formed on a plain delta wing.

References

1) Rao, D.M., "Leading-Edge Vortex-Flap Experiments on a 74 Deg. Delta wing," NASA CR-159161, Nov. 1979.

2) Campbell, J.F. and Osborn, R.F., "Leading-Edge Vortex Research: Some Nonplanar Concepts and Current Challenges," *Vortex Flow Aerodynamics Volume I*, NASA CP-2416, Jul. 1986, pp.31-63.

3) Rinoie, K., "Studies of Vortex Flaps for Different Sweepback Angle Delta Wing," *Proceedings of CEAS European Forum on High Lift and Separation Control* (Bath), Mar. 1995, pp.22.1-22.8.

4) Rinoie, K. and Stollery, J.L., "Experimental Studies of Vortex Flaps and Vortex Plates," *J. Aircraft*, Vol.31, Mar.-Apr. 1994, pp.322-329.

5) Rinoie, K., Fujita, T., Iwasaki, A. and Fujieda, H., "Studies on the Optimum Flap Deflection Angle of Vortex Flaps," *Proceedings of 19th Congress of the International Council of the Aeronautical Sciences* (Anaheim), Sep. 1994, pp.1660-1667 (ICAS-94-4.5.4).

6) Fujita, T. et al., "Model Support System Using an Industrial Robot in Low-Speed Wind Tunnel," Nat. Aero. Lab. Tech. Memo. NAL-TM-666, 1994 (in Japanese).

7) Fujita, T. et al., "A Pressure Measurement Method Using Electronically Scanner Pressure Sensors (ESP) Installed in a Gust Wind Tunnel," Nat. Aero. Lab. Tech. Memo. NAL-TM-638, 1991 (in Japanese).

8) Hummel, D., "On the Vortex Formation Over a Slender Wing at Large Angles of Attack," *High Angle of Attack Aerodynamics*, AGARD CP-247, Oct. 1978, pp.15-1 - 15-17.

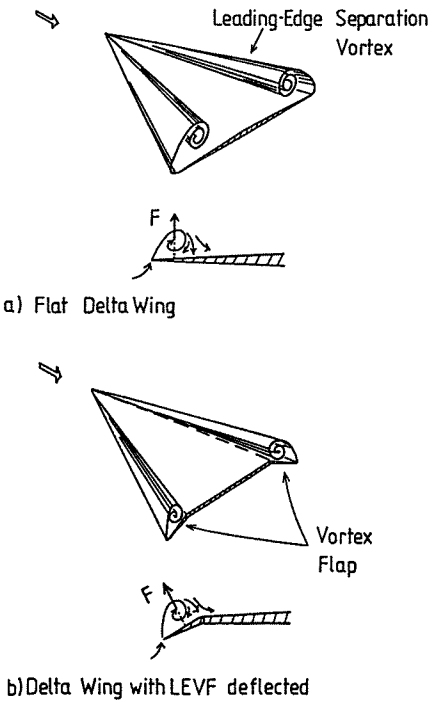

Fig.1 The Concept of a Vortex Flap[4)]

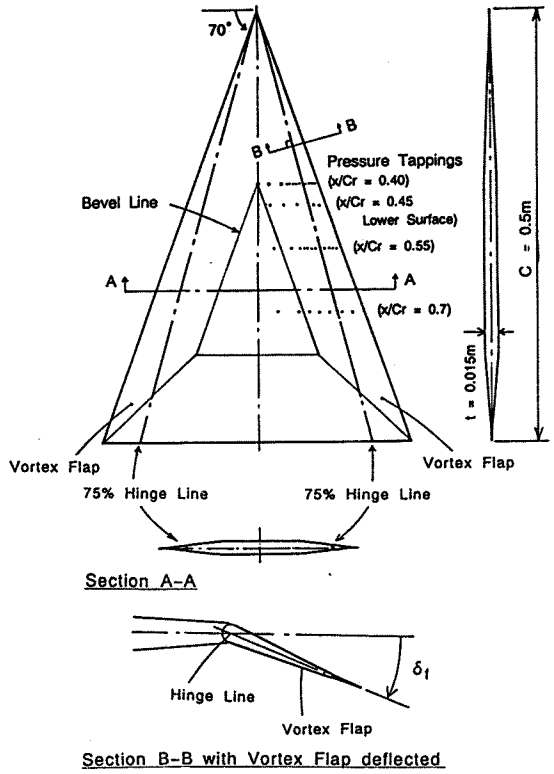

Fig.2 The 70° Delta Wing Model with LEVF[5)]

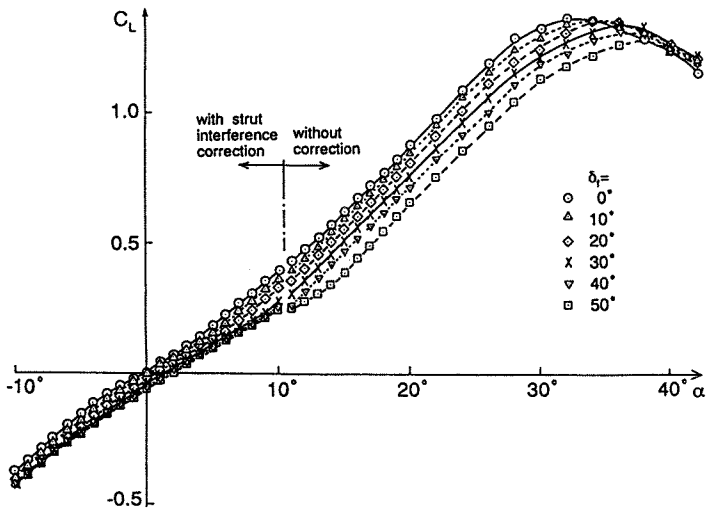

Fig.3 The Effect of the LEVF on C_L vs. α [5)]

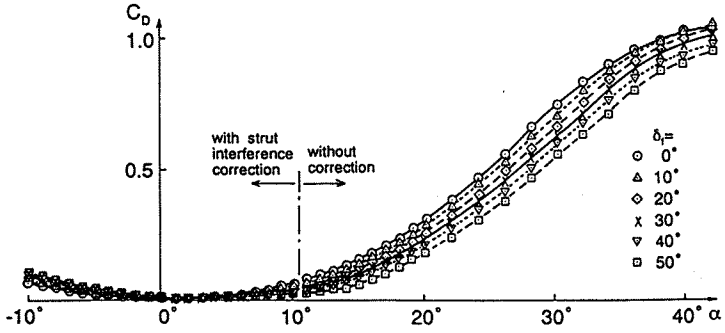

Fig.4 The Effect of the LEVF on C_D vs. α [5)]

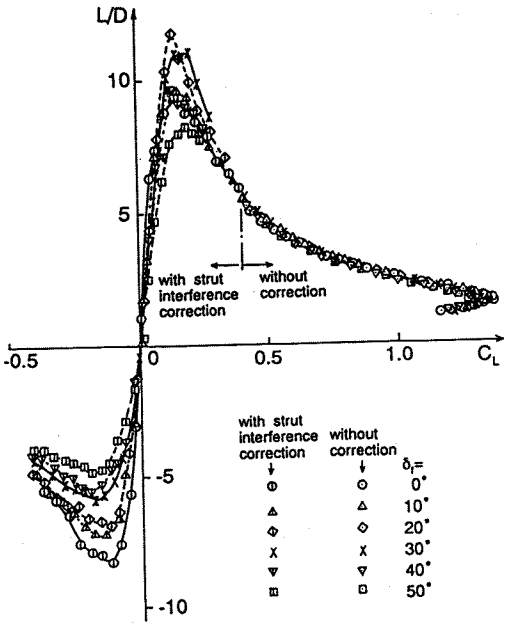

Fig.5 The Effect of the LEVF on L/D vs. C_L [5)]

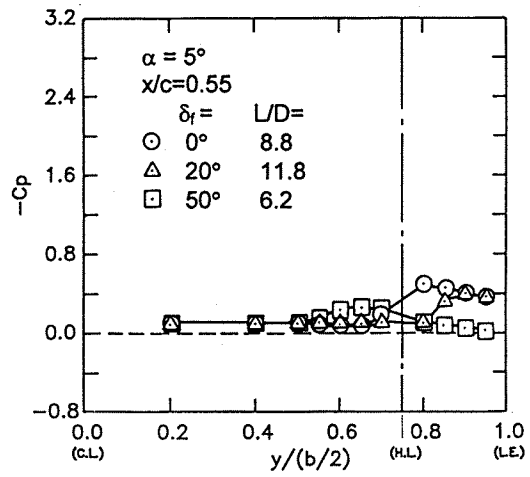

Fig.6 Surface Pressure Distributions at α=5°, x/C=0.55

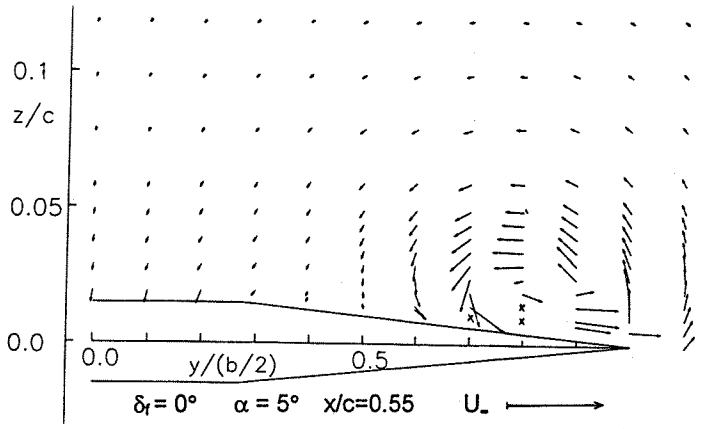

a) δ_f=0°

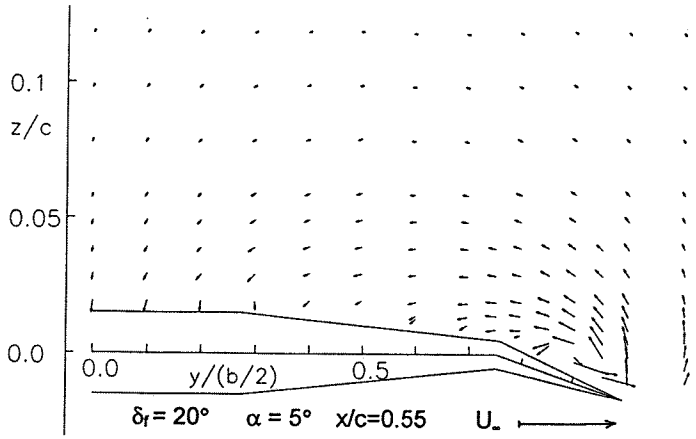

b) δ_f=20°

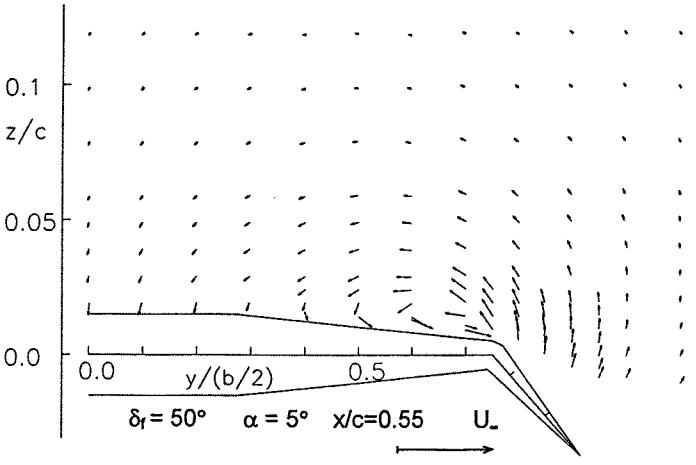

c) δ_f=50°

Fig.7 Velocity Vector Components in the Measuring Plane at α=5°, x/C=0.55

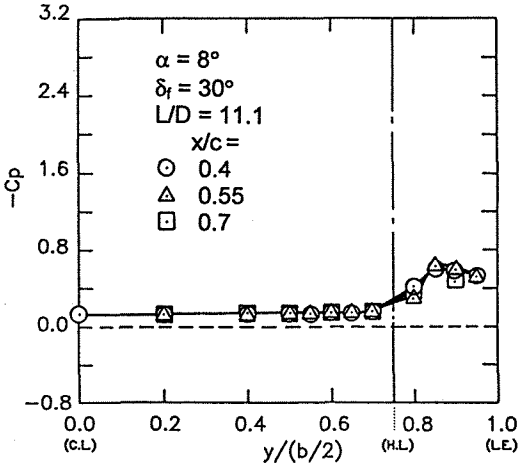

Fig.8 Surface Pressure Distributions at α=8°, δ_f=30°

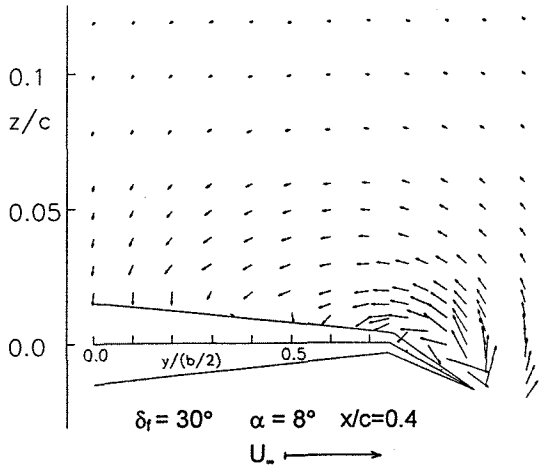

a) x/C=0.4

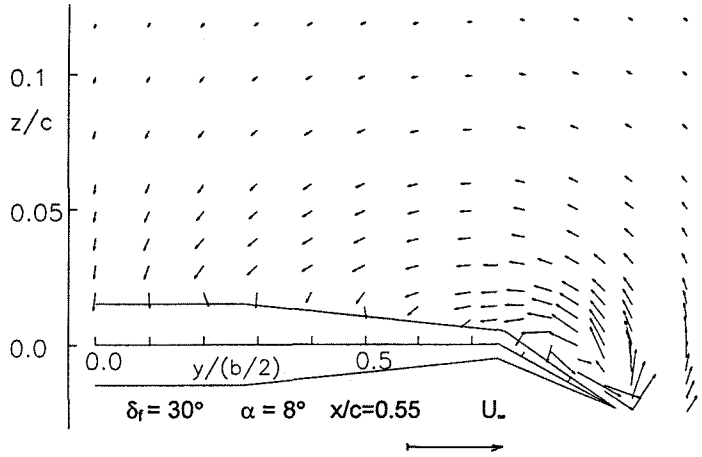

b) x/C=0.55

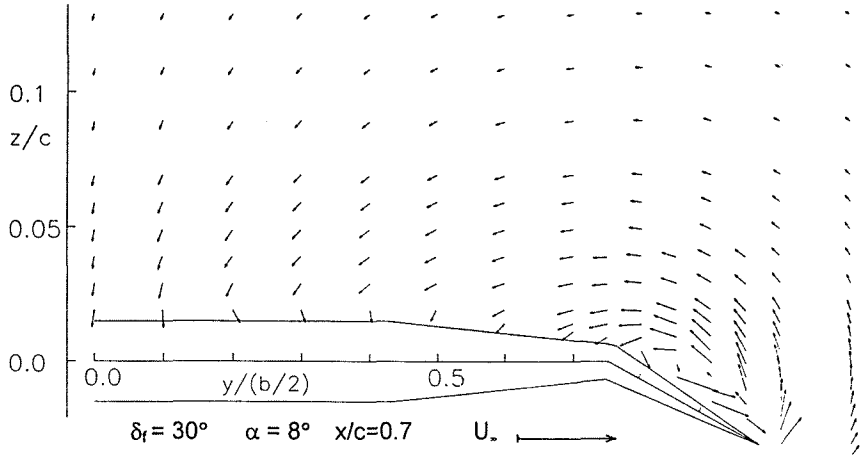

c) x/C=0.7

Fig.9 Velocity Vector Components in the Measuring Plane at α=8°, δ_f=30°

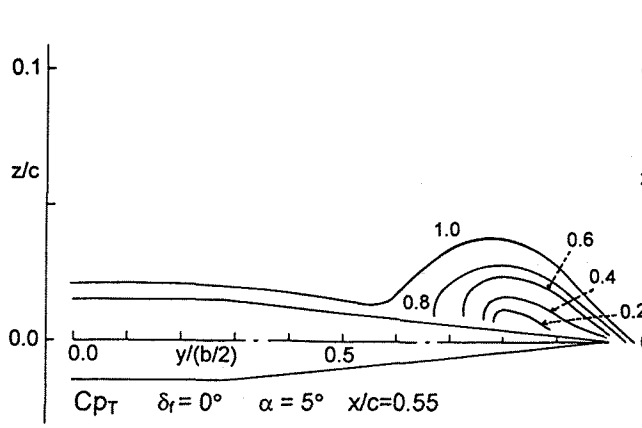

a) Total Pressure Cp_T

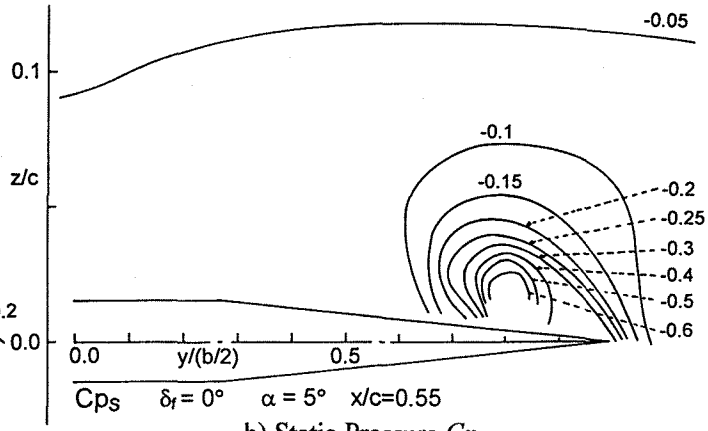

b) Static Pressure Cp_S

Fig.10 Total, Static and Dynamic Pressure Isobars at α=5°, δ_f=0°

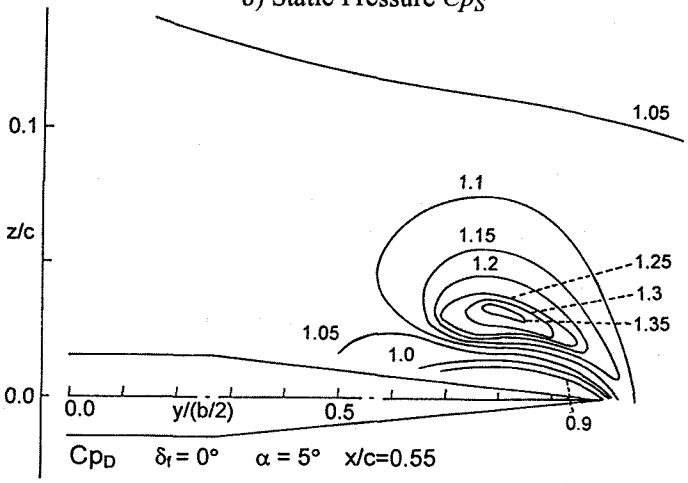

c) Dynamic Pressure Cp_D

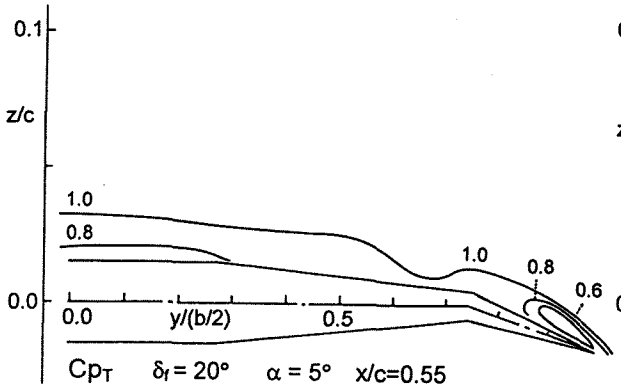

a) Total Pressure Cp_T

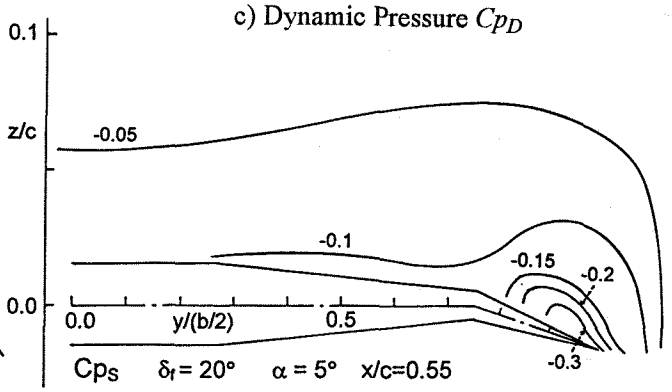

b) Static Pressure Cp_S

Fig.11 Total, Static and Dynamic Pressure Isobars at α=5°, δ_f=20°

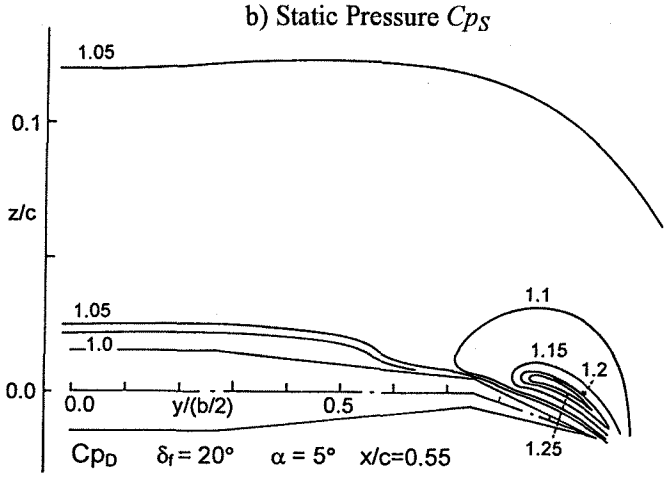

c) Dynamic Pressure Cp_D